J MATER SCI **41** (2006) 2679–2683

TEM observation of hydrogen permeable Si–M–O (M = Ni or Sc) membranes synthesized on mesoporous anodic alumina capillary tubes

S. YAMAZAKI*, N. UNO, H. MORI, Y. H. IKUHARA, Y. IWAMOTO, T. KATO, T. HIRAYAMA
Materials R&D Laboratory, Japan Fine Ceramics Center, 2-4-1 Mutsuno Atusta-ku, Nagoya 456-8587, Japan
E-mail: s-ymzk@ngk.co.jp

Published online: 17 April 2006

Microstructures of Si–M–O (M = Ni or Sc; M/Si = 0.5) membranes synthesized on a mesoporous anodic alumina capillary (MAAC) tube using chemical processing techniques were characterized by transmission electron microscopy. The chemical composition of the membranes was analyzed by energy-dispersive X-ray spectroscopy. An as-synthesized Si–Ni–O membrane was found to be formed as a thin amorphous layer with a thickness of 400 nm on the MAAC tube, and in the mesopore channels of the MAAC tube, amorphous Si–Ni–O was also formed. The EDS analysis indicated a compositional gradient of Ni/Si for the Si–Ni–O membrane. The ratio of Ni/Si increased the further in depth from the surface of the membrane. After heat treatment in a hydrogen flow, a multilayered structure was formed, and nickel and nickel oxides were precipitated in the membrane. In the Si–Sc–O membrane, neither precipitation nor compositional gradient of Sc/Si were observed. The compositional change and precipitating behaviors of the Si–Ni–O and Si–Sc–O membrane are discussed in terms of the stability of the silica-dopant metal network and the hydrogen permselectivity of the membranes.

1. Introduction

Microporous ceramic membranes have great potential for gas separation, owing to their excellent thermochemical stability. In addition, microporous ceramic membranes can be expected to be used in catalytic membrane reactors for hydrogen production [1–5]. Hydrogen-permselective amorphous silica (Si–O) membranes, having a molecular sieve-like property, have been synthesized using a sol-gel method [5–11] or a chemical vapor deposition (CVD) method [4, 12–16]. However, in order to use the amorphous Si–O membranes in such high-temperature membrane reactors, these membranes need to improve in hydrogen permselectivity and hydrothermal stability. Recently, amorphous Si–O membranes doped with nickel or scandium (Si–Ni–O or Si–Sc–O) were synthesized using a chemical solution method [17, 18]. Hydrogen permeance of the Si–Ni–O (Ni/Si = 0.5) membrane at 773 K was 1.4×10^{-7} mol $m^{-2}s^{-1}Pa^{-1}$ and the permeance ratio of H_2/N_2 and H_2/He were measured to be 84 and 5, respectively [17]. Since the H_2/He permeance ratio increased by increasing the Ni/Si ratio from 0.1 to 0.5, the doped Ni could take an important role in the selective enhancement of the hydrogen permeance of the Si–Ni–O membranes. On the other hand, hydrogen permeance of the Si–Sc–O (Sc/Si = 0.5) membrane at 773 K in 75 kPa H_2O was 1.5×10^{-8} mol $m^{-2}s^{-1}Pa^{-1}$ and H_2/N_2 permeance ratio was around 800 [18]. This hydrogen selectivity is excellent among the silica membranes since the silica membranes decreased their hydrogen selectivity after hydrothermal treatment [19]. Although the unique hydrogen permselectivity of both the Si–Ni–O and the Si–Sc–O membranes may be related to the microstructures of the membranes, there is little information about the microstructure of these membranes. In this study, the

*Present Address: Materials Research Laboratory, NGK Insulators, Ltd., 2-56 Suda-cho Mizuho-ku, Nagoya 467-8530, Japan.
0022-2461
DOI: 10.1007/s10853-006-7870-3

microstructural characterizations of the Si–M–O (M = Ni or Sc) membranes are performed using a transmission electron microscope (TEM). The chemical composition of the membranes was analyzed by energy-dispersive X-ray spectroscopy (EDS). The relationship between the microstructures and the hydrogen permselectivity of the Si–Ni–O and Si–Sc–O membranes are discussed.

2. Experimental

2.1. Membrane synthesis

All the membranes were fabricated on a mesoporous anodic alumina capillary (MAAC) tube using chemical processing techniques [17, 18]. The MAAC tube was prepared in our laboratory, and details of the fabrication are reported elsewhere [20]. The inner and outer diameters of the MAAC tubes are about 3 and 4 mm, respectively. A typical cross-sectional TEM image of a MAAC tube is shown in Fig. 1. The highly oriented and radial mesopore channels can be seen in the micrograph. The different contrast regions in the MAAC tube indicate the different diameters of the mesopore channel; region 1A in Fig. 1 has a diameter of 3–4 nm, region 1B with 6 nm and region 1C with about 16 nm [20].

Tetraethoxysilane (TEOS) was used as the source of silica, and a nickel nitrate or scandium nitrate solution was used as the source of the metal dopant. All the compounds, with a metal/silicon (M/Si) ratio of 0.5, were mixed with ethanol and hydrogen peroxide. A MAAC tube was dipped in the precursor solution, dried at room temperature and then heated at 873 K in air. This procedure was repeated several times to synthesize the Si–M–O membrane. The as-synthesized Si–Ni–O membrane was heat-treated at 773 K in a hydrogen flow for 2 h [17], while the as-synthesized Si–Sc–O membrane was hydrothermally-treated at 773 K in 75 kPa H_2O [18].

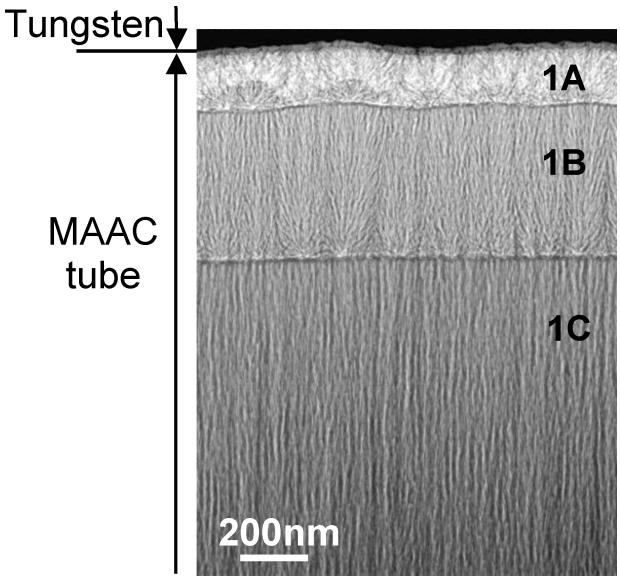

Figure 1 Cross-sectional TEM image of a MAAC tube.

2.2. Characterization by TEM

A focused-ion-beam (FIB) method is more suitable the for preparation of thin multilayered structural specimens and porous materials for TEM [21]. In this study, the TEM specimens were prepared using FIB micro-sampling [22] in a Hitachi FB2100 at an accelerating voltage of 40 to 10 kV. Tungsten was deposited on the surface of the sampling area in the FIB system to protect the top layer of the membrane from gallium ion spattering during FIB milling. The membranes were removed by FIB milling and small specimens (3 μm $\times$ 25 μm $\times$ 15 μm) were prepared. The specimens were lifted out using a tungsten needle and transferred to TEM grids. The specimens were then fixed onto the TEM grid by FIB-assisted deposition, and thinned by FIB milling. The microstructure of the Si–M–O membranes were characterized by a JEOL 2010 and a TOPCON EM-002B at an accelerating voltage of 200 kV, and the chemical compositions of the membranes were analyzed by TEM-EDS using a Noran Vantage system attached to the TOPCON EM-002B.

3. Results and discussion

3.1. Si–Ni–O membranes

A cross-sectional TEM image of an as-synthesized membrane is shown in Fig. 2 with a selected-area diffraction

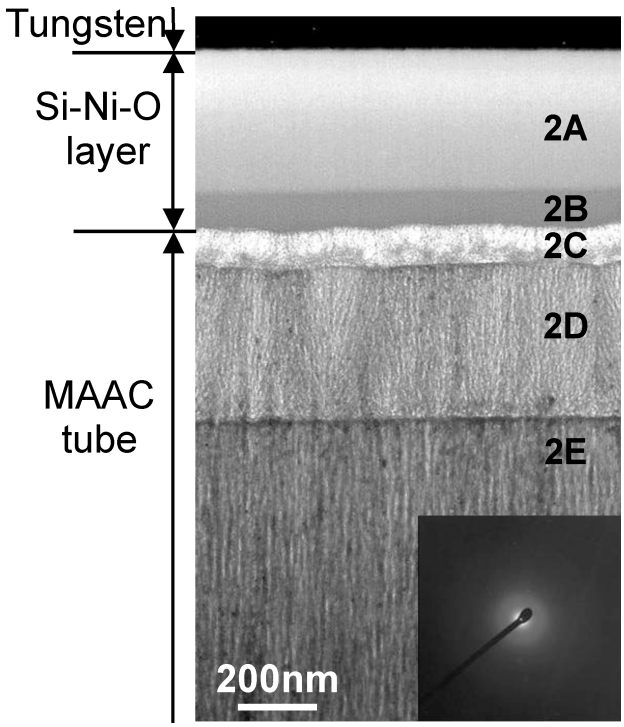

Figure 2 Cross-sectional TEM image of an as-synthesized Si–Ni–O membrane. Inset shows a selected area diffraction pattern from the Si–Ni–O layer.

pattern from the Si–Ni–O layer indicating amorphous material. The amorphous Si–Ni–O layer is located on a MAAC tube with a thickness of about 400 nm. The straight channel of the MAAC tube can be seen in the Fig. 2. The results of EDS analyses from the regions 2A–D in Fig. 2 are shown in Fig. 3a–d, respectively. The amorphous layer in the vicinity of the MAAC tube has a dark contrasted region 2B in Fig. 2, with a thickness of 100 nm, which includes aluminum as shown in Fig. 3b, though the light-contrast outer region is aluminum free as shown in Fig. 3a. This suggests that the precursor solution reacted with the MAAC tube during the dipping/heat treatment processes. In addition, silicon and nickel are detected in the MAAC tube as shown in Fig. 3c and d corresponding to the region of 1A and 1B in Fig. 1, respectively. These results indicate that the Si–Ni–O precursor infiltrated through the mesopore channels of the MAAC tube. The relative intensity of Ni–Kα to Si–Kα increased with inceasing depth from the surface of the membrane. This implies that the nickel compound was not well distributed in the Si–O network in the precursor, and therefore the extricated nickel compound in the membrane leached out into the precursor solution penetrating into the membrane and condensed within the inner MAAC tube through the repetition of the dipping process.

A cross-sectional TEM image of the membrane after the hydrogen heat treatment is shown in Fig. 4, and a selected-area diffraction pattern from the Si–Ni–O layer is shown in Fig. 5. As observed in Fig. 4, during the hydrogen heat treatment, nano-sized crystalline particles about 5–10 nm in diameter are *in situ* formed both in the Si–Ni–O layer and in mesopore channels of the MAAC tube. A nano-sized particle dispersed composite structure was formed by hydrogen heat treatment. These nano-

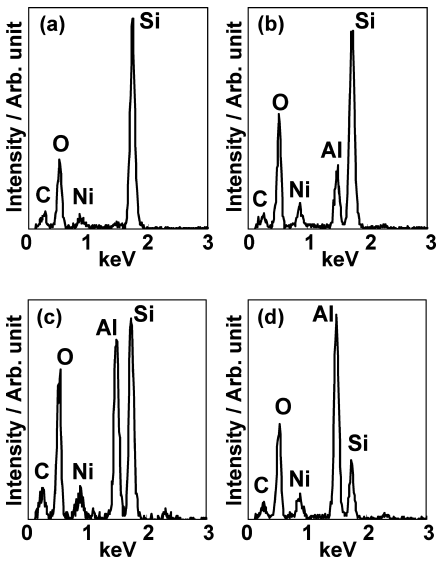

Figure 3 Results of EDS analyses from the as-synthesized Si–Ni–O membrane: the results (a)–(d) correspond to the regions 2A–D in Fig. 2, respectively.

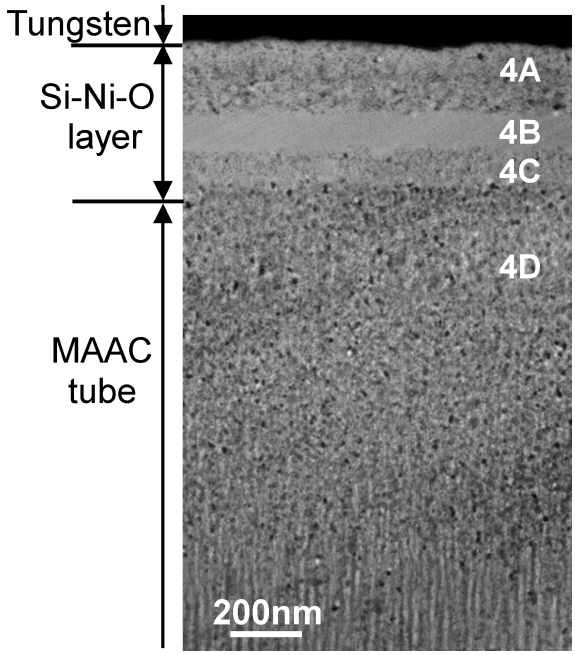

Figure 4 Cross-sectional TEM image of the hydrogen heat treated Si–Ni–O membrane.

sized particles are identified as being consistent with Ni, NiO and Ni_2SiO_4 from the diffraction pattern as shown in Fig. 5. Although the straight channel structure near the surface of the MAAC tube was damaged after the formation of nano-sized particles, the hydrogen heat-treated Si–Ni–O membrane seemed to maintain its shape, suggesting that the amorphous material formed in the MAAC tube played an important role of providing the mechanical strength of the membrane. The results of the EDS analyses from the regions 4A–D in Fig. 4 are shown in Fig. 6a–d, respectively. In the hydrogen heat-treated Si–Ni–O membrane, the gradient-like structure was observed. There is

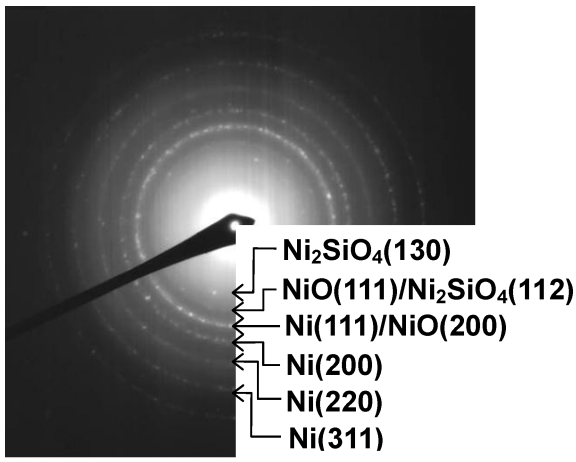

Figure 5 Selected area diffraction patterns from the Si–Ni–O layer shown in Fig. 4.

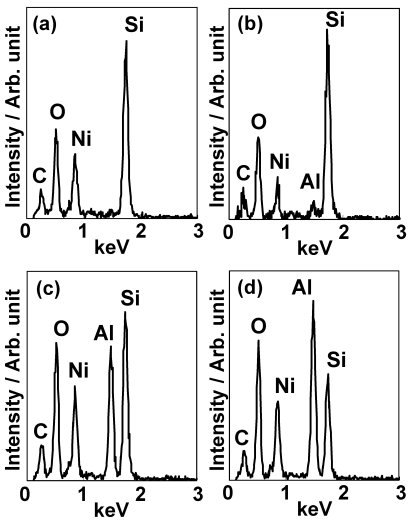

Figure 6 Results of EDS analyses from the hydrogen heat treated Si–Ni–O membrane: the results (a)–(d) correspond to the regions 4A–D in Fig. 4, respectively.

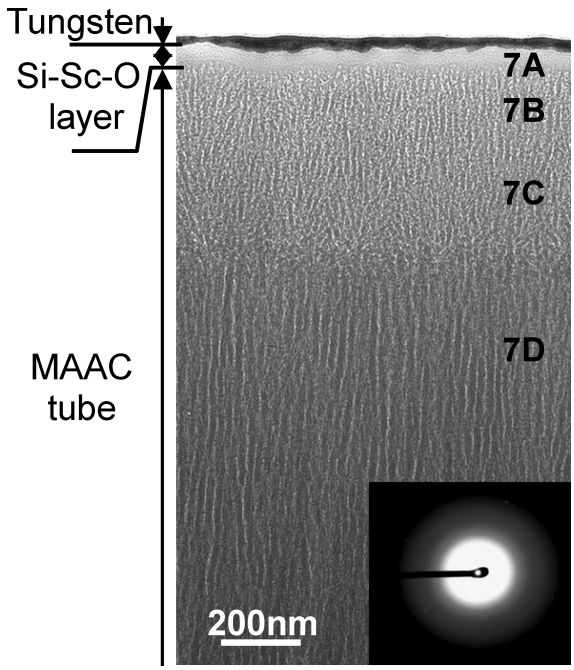

Figure 7 Cross-sectional TEM image of the hydrothermal treated Si–Sc–O membrane. Inset shows a selected area diffraction pattern from the Si–Sc–O layer and the MAAC.

a region without nano-sized particles in the membrane (region 4B) as shown in Fig. 4. The relative intensity of Ni–Kα to Si–Kα obtained from region 4B was weaker than those obtained from other regions with nano-sized particles. This means that some of the Ni compound is transferred from region 4B to other regions during hydrogen heat treatment. In a previous study, Ishikawa *et al*. [23] presented an *in situ* formation process for functional surface layers having a gradient-like structure towards the surface. It used the bleed-out phenomenon of additives intentionally mixed in the polycarbosilane. They obtained a gradient-like structure consisting of a nano-sized TiO_2-sintered surface and a nano-sized TiO_2 particle-dispersed amorphous silica matrix from the pre-ceramic polymer (polycarbosilane containing $Ti(OC_4H_9)_4$). In our Si–Ni–O membrane, it is supposed that such a bleed out phenomenon takes place.

3.2. Si–Sc–O membrane

A cross-sectional TEM image of the Si–Sc–O membrane after the hydrothermal treatment is shown in Fig. 7. The regions 7B and 7C correspond to the region 1B in Fig. 1 where a mesopore diameter is 6 nm, and the region 7D corresponds to the region 1C in Fig. 1 with a mesopore diameter of about 16 nm, respectively. The inset shows a selected-area diffraction pattern from the Si–Sc–O layer and a MAAC tube corresponding to the regions 7A and 7B in Fig. 7, respectively, indicating amorphous materials. An amorphous Si–Sc–O layer with a thickness of about 50 nm was formed on a MAAC tube. The amorphous layer is thinner than that of the Si–Ni–O membrane shown in Fig. 2 or 4. In addition, the outermost region of the MAAC tube with a mesopore diameter of 3–4 nm, corresponding to the region 1A in Fig. 1, is etched. These results indicate that the precursor solution of Si–Sc–O was different from that of Si–Ni–O in their character and reactivity with other materials, although the pH of both precursor solutions was controlled to be same. The results of the EDS analyses from the regions 7A–D in Fig. 7 are shown in Fig. 8a–d, respectively. The relative intensities of Sc–Kα to Si–Kα obtained from each region of the Si–Sc–O membrane were almost constant, and this is different from the results of Si–Ni–O membranes both prior to and after the

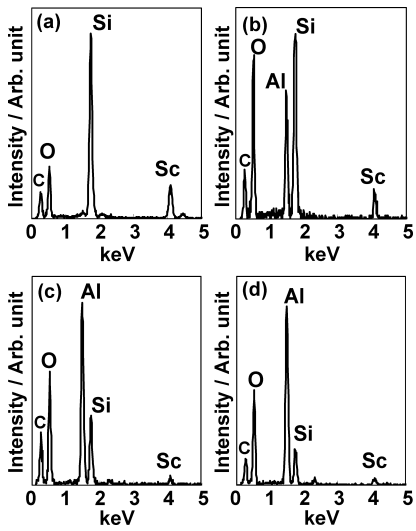

Figure 8 Results of EDS analyses from the hydrothermal treated Si–Sc–O membrane: the results (a)–(d) correspond to the regions 7A–D in Fig. 7, respectively.

hydrogen heat treatment. The constant Sc/Si composition of the membrane supports that the scandium compound was well distributed in Si–O network both in the precursor and the amorphous material, and then the condensation of scandium and precipitation of nano-sized scandium/scandium oxide were prevented. Since the stability of the amorphous silica-dopant metal network presumably depends on the kind of additive species, the stability of the amorphous Si–Sc–O network is considered to be higher than that of the Si–Ni–O. The high hydrothermal stability of the Si–Sc–O membrane might be resulted from the higher stability of the amorphous Si–Sc–O network.

4. Conclusion

The microstructures of the novel solution precursor-derived Si–M–O (M = Ni or Sc; M/Si = 0.5) membranes on a MAAC tube were characterized by TEM and the chemical compositions of the membranes were analyzed by TEM-EDS. The TEM specimens of the membranes were prepared by FIB micro-sampling. The amorphous Si–Ni–O layer was formed on the MAAC tube and the amorphous material partially filled the mesopore channels of the MAAC tube. The gradual change in the composition of Ni/Si observed for the membrane was considered to be caused by the leaching out of Ni compound from the amorphous layer followed by the condensation within the inner MAAC tube. *In situ* formation of nickel and nickel oxide nano-particles were found in the hydrogen heat-treated Si–Ni–O membrane. The composite structure composed of nickel nano-particles with hydrogen affinity and amorphous silica with a molecular sieve-like property, should achieve the selective enhancement of the hydrogen permeance. In the Si–Sc–O membrane, amorphous material was found both in and on the MAAC tube similarly to the Si–Ni–O membrane. However, the Si–Sc–O membrane kept the amorphous state after the hydrothermal treatment. The Si–Sc–O membrane with a uniform composition of Sc/Si and without phase separation suggested the stable amorphous network of Si–Sc–O, which could lead to the better performance under the hydrothermal conditions.

Acknowledgment

This work was supported by New Energy and Industrial Technology Development Organization (NEDO) as a part of the R&D Project on "Highly Efficient Ceramic Membranes for High-Temperature Separation of Hydrogen" promoted by METI, Japan.

References

1. H. M. VAN VEEN, M. BRACHT, E. HAMOEN and P. T. ALDERLIESTEN, in "Inorganic Membrane Science and Technology, Membrane Science and Technology Series," edited by A. J. Burgraaf and L. Cot (Elsevier, Amsterdam, 1996) Vol 4, p. 641.
2. K. JAROSCH and H. I. DE LASA, *Chem. Eng. Sci.* **54** (1999) 1455.
3. E. KIKUCHI, *Catal. Today* **56** (2000) 97.
4. A. K. PRABHU and S. T. OYAMA, *J. Membr. Sci.* **176** (2000) 233.
5. S. KURUNGOT, T. YAMAGUCHI and S.-I. NAKAO, *Catal. Lett.* **86** (2003) 273.
6. S. KITAO, H. KAMEDA and M. ASAEDA, *Membrane* **15**(4) (1990) 222.
7. B. N. NAIR, T. YAMAGUCHI, T. OKUBO, H. SUEMATSU, K. KEIZER and S.-I. NAKAO, *J. Membr. Sci.* **135** (1997) 233.
8. R. M. DE VOS, W. F. MAIRE and H. VERWEIJ, *ibid.* **158** (1999) 277.
9. K. YOSHIDA, Y. HIRANO, H. FUJII, T. TSURU and M. ASAEDA, *J. Chem. Eng. Jpn.* **34** (2001) 523.
10. B. N. NAIR, T. OKUBO and S.-I. NAKAO, *Membrane* **25** (2003) 73.
11. K. KUSAKABE, F. SHIBAO, G. ZHAO, K.-I. SOTOWA, K. WATANABE and T. SAITO, *J. Membr. Sci.* **215** (2003) 321.
12. G. R. GAVALAS, C. E. MEGRIS and S. W. NAM, *Chem. Eng. Sci.* **44** (1989) 1829.
13. M. TSAPATSIS and G. R. GAVALAS, *J. Membr. Sci.* **87** (1994) 281.
14. S. YAN, H. MAEDA, K. KUSAKABE, S. MOROOKA and Y. AKIYAMA, *Ind. Eng. Chem. Res.* **33** (1994) 2096.
15. G.-J. HWANG, K. ONUKI, S. SHIMIZU and H. OHYA, *J. Membr. Sci.* **162** (1999) 83.
16. M. NOMURA, K. ONO, S. GOPALAKRISHNAN, T. SUGAWARA and S.-I. NAKAO, *ibid.* (in press).
17. Y. H. IKUHARA, H. MORI, Y. IWAMOTO, N. UNO, S. YAMAZAKI and T. SAITO, *J. Mater. Res.* (submitted).
18. H. MORI, T. INADA and Y. IWAMOTO, JP patent 2004-090662.
19. M. ASAEDA and M. KASHIMOTO, in Proceedings of the Fifth International Conference Inorganic Membranes (Nagoya, 1998) p. A-405.
20. T. INADA, N. UNO, T. KATO and Y. IWAMOTO, *J. Mater. Res.* **20** (2005) 114.
21. T. KATO, Y. SASAKI, K. OSADA, T. HIRAYAMA and H. SAKA, *Surf. Interf. Anal.* **31** (2001) 409.
22. T. OHNISHI, H. KOIKE, T. ISHITANI, S. TOMIMATSU, K. UMEMURA and T. KAMINO, in Proceedings of the 25th International Symposium for Testing and Failure Analysis (Santa Clara, November 1999) p. 449.
23. T. ISHIKAWA, H. YAMAOKA, Y. HARADA, T. FUJII and T. NAGASAWA, *Nature* **416** (2002) 64.